A lossless earth Green's function representation between any two subsurface points from surface reflection GPR data

Evert Slob and Kees Wapenaar
Department of Geoscience & Engineering, Delft University of Technology
Stevinweg 1, 2628 CN, Delft, The Netherlands
e.c.slob@tudelft.nl, c.p.a.wapenaar@tudelft.nl

***Abstract*—We present a three-dimensional scheme that can be used to compute the electromagnetic impulse response between any two subsurface points from surface reflection data measured at a single surface of a lossless medium. The scheme first computes a virtual vertical radar profile using the Marchenko scheme from which focusing wavefields are computed. With the aid of the Green's functions of the virtual vertical radar profiles these focusing wavefields are then used to compute the Green's function between any two points in the subsurface. One point is a virtual receiver and the other point is a virtual source. Virtual radar images can be created as well as the whole time evolution of the radar wave field in the whole subsurface generated by one virtual source. We show with a numerical example that the method works well in a one-dimensional configuration.**

***Index Terms*—virtual source, virtual receiver, interferometry, autofocusing, 3D GPR.**

I. Introduction

Virtual receivers can be placed inside an acoustic scattering medium without having a physical source at the location of the virtual receiver [1], [2]. For ground-penetrating radar the theory for the electric and magnetic field in the earth impulse responses at virtual subsurface receiver locations were derived in [3] assuming a lossless earth model. These Green's functions of virtual vertical radar profiles can be obtained in 1D without any model information and in 3D with limited model information. The required information in 3D is that travel time from a source location at the measurement surface to the virtual receiver location inside the scattering medium must be estimated from the data, which requires some velocity analysis similar to what is done for standard imaging. For ground-penetrating radar it is important to include conductivity or more general dissipation/dispersion effects, for which a general theory for acoustic waves and electromagnetic waves can be found in [4], [5]. Retrieving virtual vertical radar profiles in a dissipative medium requires access at two side of the medium and the full scattering matrix as input data. Retrieving up- and downgoing parts of the Green's function for a virtual receiver inside the earth allows for creating an image that is free from artefacts. Such artefacts would occur when the measured surface reflection response would be used to make an image using a standard (model-driven) migration scheme [6]–[8] or linearised inversion [9].

A next step is creating the Green's functions between any two points in the subsurface. These are of relevance for holography, imaging, inverse scattering, and Green's function retrieval from ambient noise. A general unified theory was developed in [10] that can be used e.g., for acoustic, electromagnetic, and elastic wavefield applications. Here we derive the electromagnetic Green's function representation for a virtual source and a virtual receiver both located in the subsurface. We show how these virtual earth impulse responses can be obtained form the measured reflection response on the earth surface in a multi-source, multi-receiver acquisition configuration. We restrict ourselves to lossless media to be able to work with the surface reflection response only. The representations are given in the frequency domain, but are valid in the time domain. To this end, we define the time-Fourier transform of a space-time dependent vector-quantity as $\hat{\boldsymbol{u}}(\boldsymbol{x},\omega) = \int_{t=0}^{\infty}\exp(-\mathrm{j}\omega t)\boldsymbol{u}(\boldsymbol{x},t)\mathrm{d}t$, where j is the imaginary unit, ω denotes angular frequency, and $\boldsymbol{x}$ is the position vector in three-dimensional space. In the space-frequency domain the electromagnetic field vector $\hat{\boldsymbol{u}}$ is given by $\hat{\boldsymbol{u}}^t(\boldsymbol{x},\omega) = (\hat{\boldsymbol{u}}_1^t(\boldsymbol{x},\omega),\hat{\boldsymbol{u}}_2^t(\boldsymbol{x},\omega)) = \Big((\hat{E}_x,\hat{E}_y)^t,(\hat{H}_y,-\hat{H}_x)^t\Big)$, with $\hat{E}_x(\boldsymbol{x},\omega)$ and $\hat{H}_x(\boldsymbol{x},\omega)$ being the x-components of the electric and magnetic field vectors and the superscript t denotes transposition. The domain $\mathbb{D}$ is bounded by measurement surfaces at two depth levels given by $\partial\mathbb{D}_0$ at $z=z_0$ and $\partial\mathbb{D}_m$ at $z=z_m$, the focusing depth level $\partial\mathbb{D}_i$ is at $z=z_i$ with $z_0<z_i<z_m$. In what follows the physical sources are outside the domain $\mathbb{D}$. Hence inside $\mathbb{D}$ the Maxwell equations can be written as

$$\partial_3\begin{pmatrix}\hat{\boldsymbol{u}}_1\\ \hat{\boldsymbol{u}}_2\end{pmatrix} = \begin{pmatrix}\mathbf{0} & \hat{\mathbf{M}}_1\\ \hat{\mathbf{M}}_2 & \mathbf{0}\end{pmatrix}\begin{pmatrix}\hat{\boldsymbol{u}}_1\\ \hat{\boldsymbol{u}}_2\end{pmatrix}, \tag{1}$$

with material paramater operator matrices given by

$$\hat{\mathbf{M}}_1 = \begin{pmatrix}-\zeta+\partial_x\eta^{-1}\partial_x & \partial_x\eta^{-1}\partial_y\\ \partial_y\eta^{-1}\partial_x & -\zeta+\partial_y\eta^{-1}\partial_y\end{pmatrix}, \tag{2}$$

$$\hat{\mathbf{M}}_2 = \begin{pmatrix}-\eta+\partial_y\zeta^{-1}\partial_y & -\partial_y\zeta^{-1}\partial_x\\ -\partial_x\zeta^{-1}\partial_y & -\eta+\partial_x\zeta^{-1}\partial_z\end{pmatrix}, \tag{3}$$

where $\eta=\mathrm{j}\omega\varepsilon$ and $\zeta=\mathrm{j}\omega\mu$. Notice that $\hat{\boldsymbol{M}}_n^t=\hat{\boldsymbol{M}}_n$ and $\hat{\boldsymbol{M}}_n^\dagger=-\hat{\boldsymbol{M}}_n$, for $n=1,2$, and where the superscript $\dagger$ means complex conjugation and transposition.

II. Green's function representation for vertical source and virtual receiver

At any location in between the outer depth levels of $\mathbb{D}$ we can write the horizontal components of the electric field as up- and downgoing electric wavefields according to [3]

$$\hat{\boldsymbol{u}}_1 = \hat{\boldsymbol{u}}_1^+ + \hat{\boldsymbol{u}}_1^-, \tag{4}$$

where $\hat{\boldsymbol{u}}_1^+$ denotes the downgoing and $\hat{\boldsymbol{u}}_1^-$ denotes the upgoing electric field components and a similar expression can be used for the magnetic field. The horizontal components of the electric and magnetic field vectors can be written in terms of the up- and downgoing magnetic and electric fields as [11]

$$\hat{\boldsymbol{u}}_1 = \hat{\boldsymbol{M}}_2^{-1}\partial_z(\hat{\boldsymbol{u}}_2^+ + \hat{\boldsymbol{u}}_2^-), \tag{5}$$

$$\hat{\boldsymbol{u}}_2 = \hat{\boldsymbol{M}}_1^{-1}\partial_z(\hat{\boldsymbol{u}}_1^+ + \hat{\boldsymbol{u}}_1^-). \tag{6}$$

Following the procedure in [3] we apply the reciprocity theorem of the convolution and correlation types to wavefields in the same medium. Exploiting the separation in up- and downgoing waves we can select to use only electric field measurements by Following a procedure similar to the one given in Appendix C in [12] we assume that the permeability and permittivity at the depth levels z_0 and z_i are continuously differentiable in horizontal direction, then we find

$$\begin{aligned}&\int_{\partial\mathbb{D}_0}\Big[(\hat{\boldsymbol{u}}_{2;A}^+)^t\hat{\boldsymbol{u}}_{1;B}^- + (\hat{\boldsymbol{u}}_{2;A}^-)^t\hat{\boldsymbol{u}}_{1;B}^+\Big]\,\mathrm{d}^2\boldsymbol{x}\\ &= -\int_{\partial\mathbb{D}_i}\Big[(\hat{\boldsymbol{u}}_{1;A}^-)^t\hat{\boldsymbol{u}}_{2;B}^+ + (\hat{\boldsymbol{u}}_{1;A}^+)^t\hat{\boldsymbol{u}}_{2;B}^-\Big]\,\mathrm{d}^2\boldsymbol{x},\end{aligned} \tag{7}$$

and

$$\begin{aligned}&\int_{\partial\mathbb{D}_0}\Big[(\hat{\boldsymbol{u}}_{2;A}^+)^\dagger\hat{\boldsymbol{u}}_{1;B}^+ + (\hat{\boldsymbol{u}}_{2;A}^+)^\dagger\hat{\boldsymbol{u}}_{1;B}^+\Big]\,\mathrm{d}^2\boldsymbol{x}\\ &= -\int_{\partial\mathbb{D}_i}\Big[(\hat{\boldsymbol{u}}_{1;A}^+)^\dagger\hat{\boldsymbol{u}}_{2;B}^+ + (\hat{\boldsymbol{u}}_{1;A}^+)^\dagger\hat{\boldsymbol{u}}_{1;B}^+\Big]\,\mathrm{d}^2\boldsymbol{x}.\end{aligned} \tag{8}$$

In equation (8) an additional approximation is made by ignoring evanescent waves at depth levels z_0 and z_i.

State A represents the focusing wavefield where the electric field focuses at the location $\boldsymbol{x}_i$ at depth z_i and its up and downgoing components of the magnetic field are at the level $\partial\mathbb{D}_0$ in the time domain represented as $\boldsymbol{f}_1^{\pm}(\boldsymbol{x}_0, \boldsymbol{x}_i, t)$ as shown in Figure 1. The wavefields in State B are the electric reflection response generated by an electric current source at the measurement surface and the upgoing and downgoing parts of the magnetic field impulse response, or Green's function, at the focusing level as shown in Figure 2. In both states we work with two vector components of the fields and each can be generated by either of the horizontal source components, hence all fields are 2×2 matrices.

Using these wavefields in equations (7) and (8) results in

$$\begin{aligned}&\int_{\partial\mathbb{D}_0}[\hat{\boldsymbol{f}}_1^+(\boldsymbol{x}_0, \boldsymbol{x}_i, \omega)]^t\hat{\boldsymbol{R}}(\boldsymbol{x}_0, \boldsymbol{x}_0', \omega)\mathrm{d}\boldsymbol{x}_0 - [\hat{\boldsymbol{f}}_1^-(\boldsymbol{x}_0', \boldsymbol{x}_i, \omega)]^t\\ &\qquad = \hat{\boldsymbol{G}}^-(\boldsymbol{x}_i, \boldsymbol{x}_0', \omega),\end{aligned} \tag{9}$$

$$\begin{aligned}&-\int_{\partial\mathbb{D}_0}[\hat{\boldsymbol{f}}_1^-(\boldsymbol{x}_0, \boldsymbol{x}_i, \omega)]^\dagger\hat{\boldsymbol{R}}(\boldsymbol{x}_0, \boldsymbol{x}_0', \omega)\mathrm{d}\boldsymbol{x}_0 + [\hat{\boldsymbol{f}}_1^+(\boldsymbol{x}_0', \boldsymbol{x}_i, \omega)]^\dagger\\ &\qquad = \hat{\boldsymbol{G}}^+(\boldsymbol{x}_i, \boldsymbol{x}_0', \omega),\end{aligned} \tag{10}$$

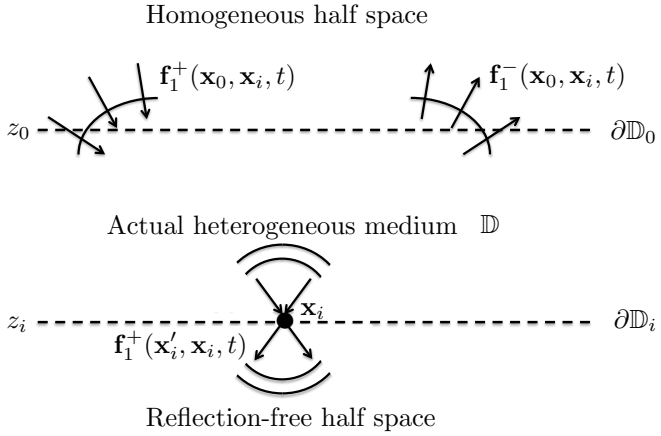

Fig. 1. State A: The focusing wavefield $\boldsymbol{f}_1^{\pm}$ at the different depth levels.

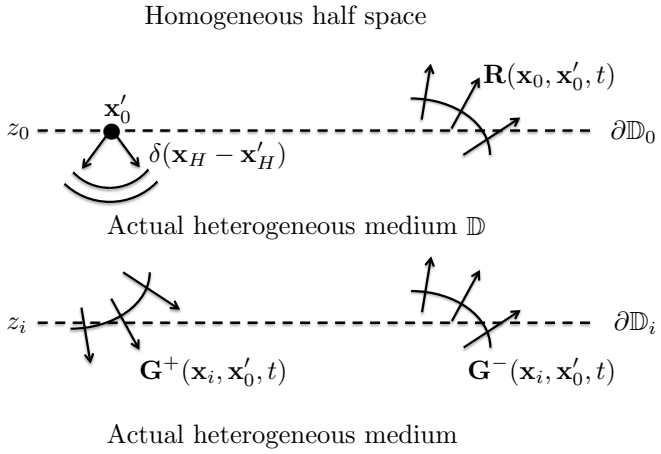

Fig. 2. State B: The actual wavefield consists of a downgoing source wavefield and its corresponding reflection response $\boldsymbol{R}$ at the depth level z_0 and the up- and downgoing parts of the electric field impulse response (Green's function) at depth level z_i.

Equations (9) and (10) represent, respectively, the upgoing and downgoing magnetic field impulse responses at a virtual receiver location $\boldsymbol{x}_i$, generated by an electric current dipole source at $\boldsymbol{x}_0'$, in terms of the measured electric field reflection response and the up- and downgoing parts of the focusing wavefield that focuses at the virtual receiver point $\boldsymbol{x}_i$. We can add both equations to find a representation for the total Green's function as (omitting the dependency on frequency for brevity)

$$\hat{\boldsymbol{G}}(\boldsymbol{x}_i, \boldsymbol{x}_0') = \int_{\partial\mathbb{D}_0}[\hat{\boldsymbol{f}}_2(\boldsymbol{x}_0, \boldsymbol{x}_i)]^t\hat{\boldsymbol{R}}(\boldsymbol{x}_0, \boldsymbol{x}_0')\mathrm{d}\boldsymbol{x}_0 + [\hat{\boldsymbol{f}}_2(\boldsymbol{x}_0', \boldsymbol{x}_i)]^\dagger, \tag{11}$$

with

$$\hat{\boldsymbol{f}}_2(\boldsymbol{x}_0, \boldsymbol{x}_i) = \hat{\boldsymbol{f}}_1^+(\boldsymbol{x}_0, \boldsymbol{x}_i) - [\hat{\boldsymbol{f}}_1^-(\boldsymbol{x}_0, \boldsymbol{x}_i)]^*. \tag{12}$$

We now proceed with a different configuration that has a magnetic current source at a location $\boldsymbol{x}_B$ in state B and we need the magnetic field Green's function $\hat{\boldsymbol{\Gamma}}$ at the level z_A and we take $z_B > z_A$ and the electric field Green's function, $\hat{\boldsymbol{\mathcal{G}}}$ at $\partial\mathbb{D}_0$. Both Green's functions correspond to

fields generated by a magnetic current source and hence at $\partial\mathbb{D}_A$ we have $\hat{\boldsymbol{u}}^{\pm}_{2;B} = \hat{\boldsymbol{\Gamma}}^{\pm}(\boldsymbol{x}_A, \boldsymbol{x}_B, \omega)$ and at $\partial\mathbb{D}_0$ we have $\hat{\boldsymbol{u}}^{-}_{1;B} = \hat{\boldsymbol{\mathcal{G}}}(\boldsymbol{x}'_0, \boldsymbol{x}_B, \omega)$ and $\hat{\boldsymbol{u}}^{+}_{1;B} = 0$. In state A we choose again the same focusing wavefields as before, but now the corresponding electric field focuses at $\boldsymbol{x}_A$ at $\partial\mathbb{D}_A$. Substituting these choices in equations (7) and (8) gives

$$\hat{\boldsymbol{\Gamma}}^{-}(\boldsymbol{x}_A, \boldsymbol{x}_B) = \int_{\partial\mathbb{D}_0} [\hat{\boldsymbol{f}}^{+}_1(\boldsymbol{x}'_0, \boldsymbol{x}_A)]^t \hat{\boldsymbol{\mathcal{G}}}(\boldsymbol{x}'_0, \boldsymbol{x}_B) \mathrm{d}\boldsymbol{x}'_0, \quad (13)$$

$$\hat{\boldsymbol{\Gamma}}^{+}(\boldsymbol{x}_A, \boldsymbol{x}_B) = -\int_{\partial\mathbb{D}_0} [\hat{\boldsymbol{f}}^{-}_1(\boldsymbol{x}'_0, \boldsymbol{x}_A)]^{\dagger} \hat{\boldsymbol{\mathcal{G}}}(\boldsymbol{x}'_0, \boldsymbol{x}_B) \mathrm{d}\boldsymbol{x}'_0. \quad (14)$$

We can add these equations, transpose both sides and use source-receiver reciprocity for both Green's functions ($[\hat{\boldsymbol{\Gamma}}(\boldsymbol{x}_A, \boldsymbol{x}_B)]^t = \hat{\boldsymbol{\Gamma}}(\boldsymbol{x}_B, \boldsymbol{x}_A), \hat{\boldsymbol{\mathcal{G}}}(\boldsymbol{x}'_0, \boldsymbol{x}_B) = -[\hat{\boldsymbol{G}}(\boldsymbol{x}_B, \boldsymbol{x}'_0)]^t$) to find the final Green's function representation

$$\hat{\boldsymbol{\Gamma}}(\boldsymbol{x}_B, \boldsymbol{x}_A) = -\int_{\partial\mathbb{D}_0} \hat{\boldsymbol{G}}(\boldsymbol{x}_B, \boldsymbol{x}'_0) \hat{\boldsymbol{f}}_2(\boldsymbol{x}'_0, \boldsymbol{x}_A) \mathrm{d}\boldsymbol{x}'_0. \quad (15)$$

These equations are valid when $z_A < z_B$. When $z_A > z_B$ we must first put the magnetic source in state B at $\boldsymbol{x}_A$ and focus at $\boldsymbol{x}_B$ and obtain

$$[\hat{\boldsymbol{\Gamma}}(\boldsymbol{x}_B, \boldsymbol{x}_A)]^t = -\int_{\partial\mathbb{D}_0} \hat{\boldsymbol{G}}(\boldsymbol{x}_A, \boldsymbol{x}'_0) \hat{\boldsymbol{f}}_2(\boldsymbol{x}'_0, \boldsymbol{x}_B) \mathrm{d}\boldsymbol{x}'_0. \quad (16)$$

Starting with the electric field reflection response measured, and generated by an electric dipole source, at the surface of a lossless medium we first use the magnetic field focusing wavefield to bring the receivers into the subsurface after which we use the same focusing wavefield to bring the sources into the subsurface. In this process we end up with the magnetic field response at any subsurface location $\boldsymbol{x}_A$ generated by a magnetic dipole at any subsurface location $\boldsymbol{x}_B$. To carry out these two steps we need to obtain the focusing wavefields $\hat{\boldsymbol{f}}^{\pm}_1$ and the procedure is described in detail in [3] and not repeated here. We suffice to say that equations (9) and (10) must be solved in the time domain in the interval where the Green's functions are zero. Once these are found equations (12) and (11) are used to compute the Green's functions $\hat{\boldsymbol{G}}$, which are then used in equations (15) and (16) to compute the Green's fucntions between any two locations in the subsurface. These can be useful in many applications including monitoring applications.

III. Numerical example

To visualise how the method works and how much data can be generated from a single data trace we look at a 1D example. The model is shown in Table I and has vertical variations in the relative permittivity ε_r. The electric source is 5 cm above the ground surface and emits a Ricker wavelet with center frequency of 250 MHz. The electric field reflection response of the medium is computed and shown in the top plot of Figure 3. We first compute the focusing functions from the data, subsequently retrieve the virtual vertical profile Green's functions, followed by the Green's functions between any two points. Equations (9) and (10) are solved in the time domain with truncations to block out the Green's function to compute

TABLE I
Layer thickness and permittivity model.

d (m)	0.05	0.60	1.75	1	∞
$\varepsilon_r(-)$	1	16	4	25	4

the focusing functions f_1 at all depth levels and they are combined in f_2 which is shown in the bottom plot of Figure 3. Comparing the top and bottom plots in Figure 3 we can see that it is possible to focus the wavefield at any depth level from a single trace of data. The vertical axis is depth, but that is just done for plotting purposes. The actual resulting focusing wavefield comes as a function of one-way travel time and in a 1D model there is no information in the data to convert those times to depth. In the bottom plot we can also see that every time we cross a boundary when we focus deeper into the model the number of events double and when we focus below the fourth and bottom reflecting boundary eight events are found in the focusing wavefield. There are 2^{n-1} events in f_1 and 2^n in f_2 for n reflectors above the focus depth.

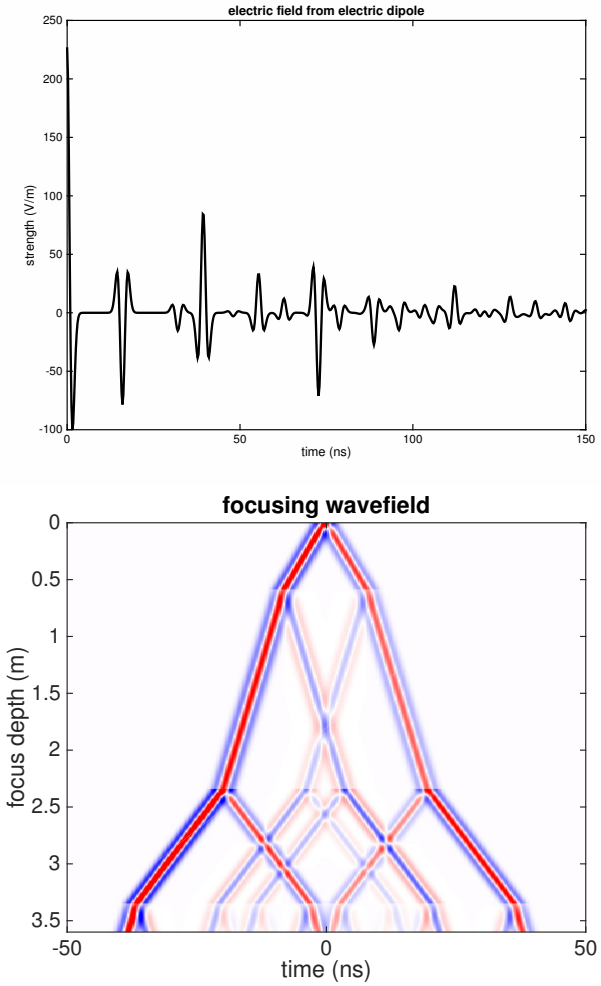

Fig. 3. The data (top) and focusing wavefield f_2 (bottom).

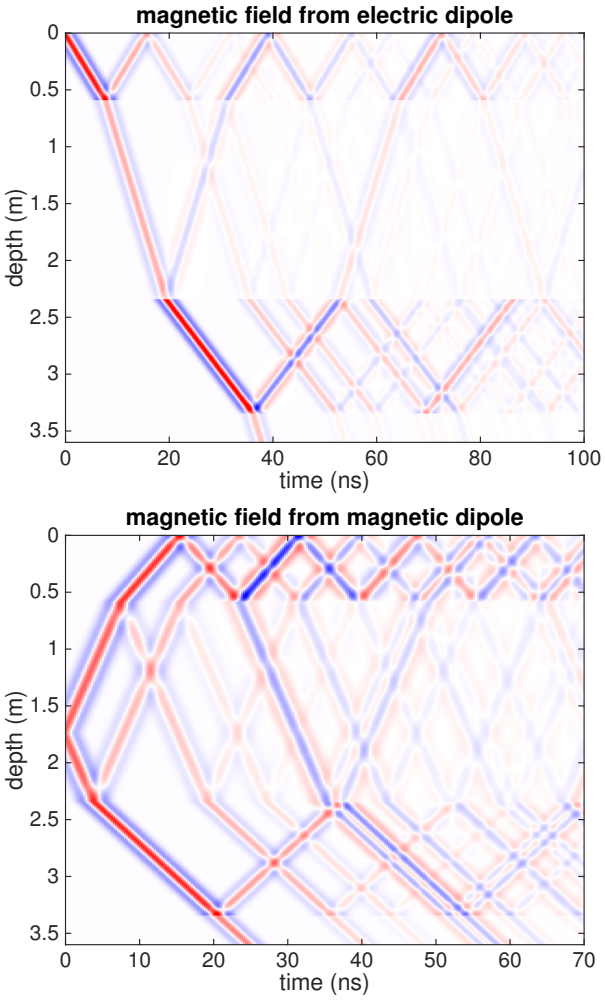

Fig. 4. Virtual source (top) and virtual source-receiver (bottom) Green's functions

Then we compute the magnetic field Green's functions for an electric dipole source at the surface in the frequency domain using equations (11) and (12) for virtual receiver positions from the surface to 0.25 m below the bottom reflector. The result is shown in the time domain for virtual receivers at all depth levels in the top plot of Figure 4. We can see from this plot that with the aid of the wavefields shown in Figure 3 we are able to make a virtual vertical radar profile at all depth levels. When this is done we have predicted the wavefield generated by electric dipole source just above the surface for receivers anywhere in the model. We then select the magnetic dipole source to be located at 1.75 m below surface, which is 1.15 m below the second reflector and compute the magnetic field Green's functions at all depth levels in the model with equations (12)-(16). The result is shown in the bottom plot of Figure 4. Hence, with the aid of the wavefield in the bottom plot of Figure 3 and the top plot of Figure 4 the wavefield shown in the bottom plot of Figure 4 is obtained. It is noted that the source can be taken anywhere in the model. We observe that from a single trace of radar data with a source and receiver just above the surface, the receiver and the source can be put at any depth level and all possible multi-source multi-receiver wavefields (data cube) can be computed.

IV. Conclusion

We have shown the theory and a numerical example to retrieve the Green's function of a virtual receiver located at a chosen position in the subsurface generated by a source at a chosen position in the subsurface. In this process the electric field reflection response generated by an electric dipole source, both located at the surface, is turned into the magnetic field generated by a magnetic dipole source, both located at arbitrary subsurface locations. The example shows that the theory works well in 1D. The next challenge is to test the method on 2D numerical data and on data measured in the laboratory or in the field. In the latter case we need to incorporate the effects of conductivity in the model.

References

[1] F. Broggini, R. Snieder, and K. Wapenaar, "Focusing the wavefield inside an unknown 1d medium: Beyond seismic interferometry," *Geophysics*, vol. 77, no. 5, pp. A25–A28, September-October 2012.

[2] K. Wapenaar, F. Broggini, E. Slob, and R. Snieder, "Three-dimensional single-sided marchenko inverse scattering, data-driven focusing, green's function retrieval, and their mutual relations," *Physical Review Letters*, vol. 110, no. 8, p. 084301, Feb 2013. [Online]. Available: http://link.aps.org/doi/10.1103/PhysRevLett.110.084301

[3] E. Slob, J. Hunziker, J. Thorbecke, and K. Wapenaar, "Creating virtual vertical radar profiles from surface reflection Ground Penetrating Radar data," in *Proceedings of the 15th International Conference on Ground Penetrating Radar (GPR2014)*, S. Lambot, A. Giannopoulos, L. Pajewski, F. Andre, E. Slob, and C. Craeye, Eds. 345 E 47th St, New York, NY 10017, USA: IEEE, 2014, pp. 525–528.

[4] E. Slob, "Green?s Function Retrieval and Marchenko Imaging in a Dissipative Acoustic Medium," *Physical Review Letters*, vol. 116, no. 16, April 2016.

[5] E. Slob and L. Zhang, "Electromagnetic marchenko equations for a dissipative heterogeneous medium," in *Proceedings of the 2016 16th International Conference on Ground Penetrating Radar (GPR)*. 345 E 47th St, New York, NY 10017, USA: IEEE, 2016.

[6] M. Grasmueck, R. Weger, and H. Horstmeyer, "Full-resolution 3d gpr imaging," *Geophysics*, vol. 70, no. 1, pp. K12–K19, Jan-Feb 2005.

[7] G. Gennarelli and F. Soldovieri, "Multipath ghosts in radar imaging: Physical insight and mitigation strategies," *IEEE Journal of Selected Topics in Applied Earth Observations and Remote Sensing*, vol. 8, no. 3, pp. 1078–1086, Mar 2015.

[8] E. R. Almeida, J. L. Porsani, I. Catapnaio, G. Gennarelli, and F. Soldovieri, "Microwave tomography-enhanced gpr in forensic surveys: The case study of a tropical environment," *IEEE Journal of Selected Topics in Applied Earth Observations and Remote Sensing*, vol. 9, no. 1, pp. 115–124, Jan 2016.

[9] G. Gennarelli, I. Catapano, F. Soldovieri, and R. Persico, "On the achievable imaging performance in full 3-d linear inverse scattering," *IEEE Transactions on Antennas and Propagation*, vol. 63, no. 3, pp. 1150–1155, Mar 2015.

[10] K. Wapenaar, J. van der Neut, and E. Slob, "Unified double- and single-sided homogeneous Green's function representations," *Proceedings of the Royal Society A-Mathematical Physical and Engineering Sciences*, vol. 472, no. 2190, June 2016.

[11] E. Slob, "Interferometry by deconvolution of multi-component multi-offset gpr data," *IEEE Trans. Geoscience and Remote Sensing*, vol. 47, no. 3, pp. 828–838, March 2009.

[12] C. P. A. Wapenaar and A. J. Berkhout, *Elastic wave field extrapolation: Redatuming of single- and multi- component seismic data*, ser. Advances in Exploration Geophysics. Elsevier Science Publishers, 1989.

[13] K. Wapenaar, J. Thorbecke, J. van der Neut, F. Broggini, E. Slob, and R. Snieder, "Marchenko imaging," *Geophysics*, vol. 79, no. 3, pp. WA39–WA57, May-June 2014.